https://doi.org/10.5194/wcd-2021-72
Preprint. Discussion started: 15 November 2021


# Regime transitions of Australian climate and climate extremes

Jorgen S. Frederiksen[1,2], Stacey L. Osbrough[1,2]

[1]CSIRO Oceans and Atmosphere, Aspendale, 3195, Australia
[2]Monash University, Clayton, 3800, Australia

*Correspondence to*: Jorgen S. Frederiksen (jorgen.frederiksen@csiro.au)

**Abstract.** Systematic changes, since the beginning of the 20th century, in average and extreme Australian rainfall and temperatures indicate that Southern Australian climate has undergone regime transitions into a drier and warmer state. South-west Western Australia (SWWA) experienced the most dramatic drying trend with average streamflow into Perth dams, in the last decade, just 20% of that before the 1960s and extreme, decile 10, rainfall reduced to near zero. In south-eastern Australia (SEA) systematic decreases in average and extreme cool season rainfall became evident in the late 1990s with a halving of the area experiencing average decile 10 rainfall in the early 21st century compared with that for the 20th century. The shift in annual surface temperatures over SWWA and SEA, and indeed for Australia as a whole, has occurred primarily over the last 20 years with the percentage area experiencing extreme maximum temperatures in decile 10 increasing to an average of more than 45% since the start of the 21st century compared with less than 3% for the 20th century mean. Average maximum temperatures have also increased by circa 1ºC for SWWA and SEA over the last 20 years. The climate changes are associated with atmospheric circulation shifts and are indicative of second order regime transitions, apart from extreme temperatures for which the dramatic increases are suggestive of first order transitions.

## 1 Introduction

Over the last seventy years, since the middle of the 20th century, aspects of Australian climate, particularly rainfall and temperatures, have undergone significant changes (CSIRO and Bureau of Meteorology, 2015; Alexander and Arblaster, 2017; Dey et al., 2019; Bureau of Meteorology and CSIRO, 2020; Osbrough and Frederiksen, 2021, hereafter OF21, review the literature). The notable rainfall deficits in southern Australia have been linked to declines in extra-tropical storminess and the intensity of explosive storms (Frederiksen and Frederiksen, 2005, 2007; Hope, 2006; Pezza et al., 2008; Frederiksen et al., 2010; Alexander et al., 2011; Pook et al., 2012; Risbey et al., 2013; Frederiksen et al., 2017; Quinting et al., 2019; OF21). Some of those changes have been quasi-cyclical due, for example, to variability associated with the El Niño-Southern Oscillation or the Indian Ocean Dipole (Cai et al., 2009; L'Heureux et al., 2017; Whelan and Frederiksen, 2017; Frederiksen and Francey, 2018; OF21 review the literature). On the other hand, there is also compelling evidence for systematic climate shifts in both hemispheres due to global warming (Corti et al., 1999; Frederiksen et al., 2010; O'Kane et al., 2013; CSIRO and Bureau of Meteorology, 2015; Franzke et al., 2015; Frederiksen and Grainger, 2015; Freitas et al., 2015; Frederiksen et al., 2017; Grose et al., 2019; Bureau of Meteorology and CSIRO, 2020; OF21).

https://doi.org/10.5194/wcd-2021-72
Preprint. Discussion started: 15 November 2021


Our particular interest in this article is whether the changes that have occurred in Australian climate and climate extremes over the last seventy years are indicative of regime transitions in a noisy environment. There has been a long history of studies examining the possibility of regime transitions in various aspects of the climate system. The early simple energy balance models (EBMs) of the earth's climate (Budyko, 1969; Sellers, 1969; Faegre, 1972; Schneider and Gal-Chen, 1973; Frederiksen, 1976; Ghil, 1976) exhibited thermodynamical regime transitions in the mean temperature between several states as the order parameter, the solar constant, is varied. Indeed, as shown in Figures 1 and 3 of Frederiksen (1976), the number of stable states and the number of bifurcation points (or critical or tipping points) may vary depending on the form of the thermodynamical functions, such as the effective albedo, and lead to the possibility of closely spaced tipping points.

Charney and Devore (1979) and Wiin-Nielsen (1979) studied low order dynamical models of the atmospheric circulation and found multiple equilibrium states dominated by either strong zonal flow and weak wave structure or weak zonal flow and strong wave structure that they interpreted as a blocking state. Charney and Devore (1979) found that regime transitions between the zonal and blocking states occurred as the order parameter, the height of the topography, varied through the bifurcation point. Similar regime transitions were also found in baroclinic models by Charney and Straus (1980). Frederiksen and Frederiksen (1989) reviewed subsequent developments in the theory of multiple equilibria and the role of topographic instability in regime transitions.

Frederiksen (1985, 1991) examined regime transitions of inviscid barotropic and baroclinic zonal flows over topography in high dimensional systems using methods of equilibrium statistical mechanics. The critical points for barotropic flow and critical lines and triple points for baroclinic flows were determined and the similarities and differences with magnetic phase transitions (Patashinski and Pokrovskii, 1979; Thompson, 1979) were examined. Zidikheri et al. (2007) studied the interaction of barotropic zonal flows with topography in high resolution forced dissipative numerical simulations and established the phase diagram (their Figure 2) for regime transitions. They found hysteresis effects in transitions between strong and weak zonal flow states with qualitative similarities to those for magnetic phase transitions (e.g., Figure 3 of Saghayezhian et al. (2019) and references therein). The regime transitions between strong zonal states and blocking found in simple models have also been found in comprehensive weather prediction models (e.g., Frederiksen et al. (2004)) and associated with observed climate shifts (O'Kane et al., 2013).

Further developments in the role of regime transitions and tipping points in various aspects of the climate system, including under global warming, have been considered by Franzke et al. (2015); Freitas et al. (2015); Jones and Ricketts (2017); Dijkstra (2019); Lenton (2019); Kypke et al. (2020); Yan et al. (2020); Fabiano et al. (2021); and Australian Academy of Science (2021). It is clear from all the studies mentioned in this Introduction that there are dynamical and thermodynamical processes of the climate system that can result in regime transitions. However, the methodologies for analysing components and simplifications of the climate system are not easily applied to the full system given its complex equations and interactions over vast scales. This is clearly the case for the analytical and semi-analytical bifurcation methods, including singularity theory (Ball, 2007), for analysing low order systems (Dijkstra, 2013) and for the equilibrium statistical mechanics methods (Frederiksen, 1985, 1991). Renormalization group methods (Wilson and Kogut, 1974; Wilson, 1979; McComb, 2004 reviews

https://doi.org/10.5194/wcd-2021-72
Preprint. Discussion started: 15 November 2021


the literature) and renormalized perturbation theory (McComb, 2004; Frederiksen, 2017 review the literature) are more generally applicable to the statistical dynamics of phase transitions but the complex equations and interactions of the climate system again make these approaches unfeasible. In this study we therefore take an approach based on the general characteristics of phase transitions which involve a discontinuity in the dependent variable (first order phase transition) or its derivative (second order phase transition) as the order parameter transits through a critical point (Harter et al., 2017; Saghayezhian et al., 2019 and references therein).

The paper is structured as follows. The mean and extreme rainfall, streamflow into Perth dams, the mean and extreme surface temperature data sets, and the reanalysis data determining atmospheric flow fields, are described in Section 2. Section 3 examines changes in SWWA mean and extreme rainfall and streamflow since the beginning of the 20$^{th}$ century and relates the changes to those of the atmospheric circulation in the surrounding regions. There, systematic shifts in these variables and their trends or gradients over different time periods are examined and are related to regime transitions. In Section 4, a corresponding analysis is performed for mean and extreme rainfall for SEA and in Section 5 results for northern Australia are presented. The changing nature of SWWA average and extreme maximum surface temperatures are examined in Section 6 and the shifts in temperatures and trends again related to transitions between regimes. Section 7 presents an analysis of temperature trends in SEA, and for states and regions fully or partially within this area, while Section 8 summarizes corresponding results for Australia as a whole. The implications of our findings and our conclusions are discussed in Section 9.

## 2 Data sets

### 2.1 Rainfall, temperature and streamflow data sets

The average and extreme rainfall and temperature data used in this paper have been obtained from the Bureau of Meteorology (2020) website. In this study we focus on various regions such as SWWA, SEA, northern Australia, and Australian states, shown in Fig. 1. The construction of the rainfall data set is described by (Jones et al., 2009) and the temperature data set by (Trewin, 2013). The data for streamflow into Pert dams has been obtained from the Water Corporation (2020) of Western Australia.

### 2.2 Reanalysis data sets

The analysis of the changes in atmospheric circulation in our study uses the reanalysis data set of the National Centers for Environmental Prediction (NCEP) and the National Centre for Atmospheric Research (NCAR), (Kalnay et al., 1996). It will be referred to as the NNR data set.

https://doi.org/10.5194/wcd-2021-72
Preprint. Discussion started: 15 November 2021


## 3 South west Western Australian rainfall, rainfall extremes and atmospheric circulation

In this section, we analyse rainfall over SWWA and streamflow into Perth dams since the early 1900s. There was a notable deficit in Southern Wet Season (SWS), April to November, rainfall in SWWA and an even larger relative reduction in annual streamflow into Perth dams between the mid-1970s and early 1980s. This has been documented in numerous studies, starting with the articles by Pittock (1988) and Sadler et al. (1988), and further analysed and reviewed by Hope (2006); Bates et al. (2008) and OF21. Frederiksen and Frederiksen (2005; 2007 - hereafter FF05, FF07) noted that there was an associated 17% reduction in the peak upper troposphere winter jet-stream and a 20% drop in the $300-700$ hPa baroclinicity in the region of SWWA between 1949-1968 and 1975-1994. They showed through instability model calculations, with the respective observed climate states for the above two 20-year periods, that there was a circa 30% reduction in the growth rate of leading storm track modes crossing SWWA and a poleward deflection of some storms. OF21 have recently confirmed, through a detailed data driven study, that the cause of the SWWA winter rainfall decrease over the last 50 years is in fact the reduction in the intensity of the fast-growing storms associated with changes in the basic state.

Our aim here is to present evidence that both SWS rainfall over SSWA and Perth annual streamflow have undergone regime transitions with qualitative similarities to the phase transitions discussed in the Introduction.

### 3.1 SWWA rainfall, rainfall extremes and streamflow

We start by examining the time series of SWS rainfall over SWWA rainfall and annual streamflow into Perth dams between January to December. The SWWA region is shown in Fig. 1 which also displays other regions of Australia that we consider in this study. Figure 2 shows the time series of (a) SWWA rainfall in SWS from 1900 to 2019, (b) the Percentage Area with Rainfall in Decile 10 ($PAR_{D10}$) for SWWA in SWS and (c) the January to December Perth streamflow from 1911 to 2018. We note that the three graphs show a general decline with time. This is perhaps most easily seen from Table 1 where averages of these quantities are displayed for different time spans. For each time interval shown the rainfall, streamflow and $PAR_{D10}$ decrease systematically apart from a slight recovery of $PAR_{D10}$ in the last period. The reductions shown there are quite profound for streamflow and extreme rainfall. We note that Perth streamflow decreased from an annual average of 414 giga litres for 1911-1958 to 389 giga litres for 1959-1978 to 183 giga litres for 1979-2018 and to as little as 88 giga litres for 2009-2018. Thus, in the last decade Perth streamflow has reduced to just 21% of the historical annual average inflow into dams. Extreme rainfall, represented by $PAR_{D10}$ in Table 1, followed a similar dramatic decrease. By these two measures the climate of SWWA has transited into a completely different regime. Somewhat lesser declines in streamflow have also occurred in other drainage divisions across southern and eastern Australia (Bureau of Meteorology and CSIRO, 2020). For SWWA rainfall (Fig. 1a) the broad decreases with time follow a similar pattern to streamflow (Fig. 1c) but with the magnitudes of the reductions being considerably less, at circa 20%, since the 1970s.

Table 2 shows correlations (and detrended correlations) for the period 1911-2018 of annual streamflow into Perth dams with SWWA rainfall and $PAR_{D10}$ for SWS. As expected from Fig. 2, the correlations are substantial. They are even somewhat larger

https://doi.org/10.5194/wcd-2021-72
Preprint. Discussion started: 15 November 2021


with the rainfall squared and with a quadratic fit of rainfall with streamflow. Annual streamflow into Perth dams is particularly well predicted or described by the quadratic fit with correlation $r = 0.88$ (detrended $r = 0.86$).

Next, we consider decadal variability of rainfall, streamflow and $PAR_{D10}$. Figure 3 shows time series of 10 year running means of these variables that make the systematic decrease since the mid 1970s more evident than the noisier annual data in Fig. 2. The close covariability of the low-pass filtered SWWA rainfall and Perth streamflow is evident and the correlations are even larger ($r = 0.94$ and detrended $r = 0.83$) than for interannual variability ($r = 0.84$ and detrended $r = 0.81$). Perhaps most dramatic is the drop in $PAR_{D10}$ displayed in Fig. 3b from before the 1970s to after. This illustrates an important point that how evident a regime transition is depends on the variable of interest and its sensitivity to the changes in the forcings or external environment (order parameters). Clearly extreme rainfall is more sensitive to changes in the circulation that in turn affect the extratropical storms and rainfall (FF07; OF21).

The nature of the regime transition can be further elucidated by examining the average trend or gradient of the rainfall and streamflow data over relevant time spans. This is summarized in Table 3 which show the trends up to 1958, between 1959 and 1978 and since 1979. For each of the data sets there is a considerable decreasing trend in the twenty years between 1959-1978 compared with in the periods before and after. Again, these results support the proposition that SWWA rainfall and streamflow into Perth dams underwent a regime transition from a relatively high rainfall state to a lower much drier state and that this occurred over a period of about twenty years. The broad findings detailed for SWS over SWWA apply equally to winter rainfall and Cool Season (April to October) rainfall (not shown).

### 3.2 SH atmospheric circulation

As noted in FF07 and further analysed and reviewed by OF21, the July rainfall reduction in SWWA after the 1970s was accompanied by significant decreases in the July upper tropospheric subtropical jet near 30°S over Australia. Here, we examine the time series of the SH jet stream changes since the mid-20th century in more detail focusing on the SWS of April to November. Figure 4 shows a latitude cross section of the (1975-1994) minus (1949-1968) zonal wind difference in the region 30°S-35°S, 100°E-130°E. It has broadly similar structure to the corresponding difference for July show in Fig. 1c of FF07. In both cases there are significant wind decreases in the upper troposphere near 35°S, with increases near 60°S and decreases again near 75°S. As well these findings are reflected in January to December annual average differences (not shown) indicating the systematic nature of the changes.

Heavy rainfall from rapid extratropical storm development (OF21 and references therein) depends on the baroclinicity of the atmosphere. Phillips (1954) formulated a simple instability criterion for storm development which may be expressed as

$$U^{upper} - U^{lower} - U^{critical} > 0$$

which is necessary for baroclinic instability. The superscripts denote the winds at appropriate upper and lower levels of the atmosphere and the critical value, $U^{critical}$, depends on the vertical temperature gradient and the Coriolis parameter. In spherical geometry the expression for $U^{critical}$ is given, for example, by Frederiksen (1978, Eq (3.9)) and in Eq. (1) of OF21 (and references therein). FF07 and Frederiksen and Frederiksen (2011 – hereafter FF11) found that the primary determinant

https://doi.org/10.5194/wcd-2021-72
Preprint. Discussion started: 15 November 2021


of changes in the SH baroclinicity during the 20th century were changes in the zonal wind shear with changes in the vertical temperature gradient, and thus in $U^{critical}$, being relatively minor.

Figure 5 shows the interannual variability of the April to November (SWS) 150 hPa zonal wind (part a) and baroclinicity measured by the $300-700$ hPa zonal wind (part b) between 30°S-35°S, 100°E-130°E and from 1948 to 2018 based on NNR data. For both the peak upper tropospheric zonal wind and the baroclinicity there is a general reduction from 1948 until the mid-1970s and thereafter there is a flattening of the running mean curve until the end of the record. These changes are further quantified in Tables 4 and 5. Table 4 show the systematic decrease in 150 hPa zonal wind and $300-700$ hPa tropospheric baroclinicity for the time spans 1948-1958, 1959-1978 and 1979-2018. The corresponding trends or gradients of these field for 1959-1978 and 1979-2018 are given in Table 5. The gradients decrease rather steeply between 1959-1978 and thereafter the trend is near zero. In these respects, the results in Table 5 mirror those for SWWA rainfall and stream flow into Perth dams shown in Table 3. The flow field results are consistent with a regime transition into a weaker zonal flow and baroclinicity state in the regions upstream and over SWWA in the twenty-year period 1959-1978. Tables 4 and 5 also show the corresponding changes in the mean values and gradients for the 700 hPa zonal wind in the region 20°S-35°S, 110°E-130°E. We note that in the lower troposphere the relative changes in the mean zonal wind values and particularly gradients are considerably weaker than in the upper troposphere.

Table 6 shows correlations between mid-tropospheric baroclinicity and characteristics of SWWA rainfall for SWS and annual streamflow into Perth dams for the time span 1959-2018; similar results are obtained for 1948-2018 (not shown). Correlations with the $300-700$ hPa zonal wind are as high as 0.58 except with $PAR_{D10}$ where they are lower. We note however that somewhat larger correlations between baroclinicity and rainfall may be obtained by optimizing the region and levels of the flow fields (OF21). This is done in the right-hand column of Table 6 where correlations (as high as 0.66) with the 700 hPa zonal wind in the region 20S-35S 100E-132.5E are shown for SWS. As noted in OF21 the strong correlations of SWWA rainfall with the low-level flow suggests that surface cyclogenesis is a major contributor to the rainfall and the variability of the 700 hPa zonal wind is a primary determinant of variability in low-level baroclinicity. Their results for July are confirmed here for the time span of April to November.

## 4 South east Australian rainfall, rainfall extremes and atmospheric circulation

Next, we examine changes in SEA rainfall since the early 1900s with a particular emphasis on indications of regime transitions as in Section 3 for SWWA rainfall. We focus on the Cool Season (CS), April to October, SEA rainfall which is most affected by extra-tropical storms (OF21). Perhaps the most dramatic period of rainfall reduction during the 20th and early 21st century was the Australian Millennium Drought (AMD) of 1997 to 2009. SEA rainfall changes, particularly during the AMD, have been the focus of numerous diagnostic studies including by Fawcett (2004); Gallant et al. (2007) and Watkins and Trewin (2007), and further investigated and reviewed by Risbey et al. (2013); Cai et al. (2014); Dey et al. (2019); and OF21. These works have established the AMD as one of the most widespread and devastating droughts of the last century. FF11 related the

https://doi.org/10.5194/wcd-2021-72
Preprint. Discussion started: 15 November 2021


changes in 1997-2006 rainfall over Southern Australia compared to the 1949-1968 base-line period to changes in the large-scale circulation and changes in the growth of weather systems. Their theoretical primitive equation calculations showed that the growth rates of leading extra-tropical storm track modes were reduced by more than 30% and onset-of blocking modes by around 20% although there was some increase in the growth rate of North-West Cloud Band modes (NWCBs) and intraseasonal oscillation modes. These theoretical analyses of the causes of the AMD were also supported by the observational study of Risbey et al. (2013), who found fewer fast growing and intense frontal storms and cut-off lows during the AMD and again attributed this to the reduction in baroclinicity in the Australian region. The data driven analysis in OF21 confirmed these findings and established that changes in the intensity of explosive storms were primarily responsible for the reduced winter rainfall in Southern Australia during the AMD. They also found that while the El Niños played a significant role in the SEA rainfall reduction during the AMD the general drying of Southern Australia continued and is evident during the longer period 1997-2016.

### 4.1 SEA rainfall and streamflow

Figure 6 shows the annual and 10 year running mean time series of SEA rainfall and extreme rainfall characterized by $PAR_{D10}$ for the Cool Season (CS) of April to October; results based on April to November (SWS) are broadly similar (not shown). The reduction in SEA rainfall and $PAR_{D10}$ are most evident from the late 1990s as also see in from Table 7. The SEA reductions in rainfall of about 10% and a halving of $PAR_{D10}$ since the late 1990s are very significant as they affect the Murray Daring Basin (MDB; see Fig. 1) which is Australia's main food bowl. Nevertheless, they are not yet as dramatic as the larger reductions experienced by SWWA since the late 1970s discussed in Section 3. As one would expect, many of the states and sub-regions making up, or overlapping with, SEA experienced very similar Cool Season changes as those depicted for SEA. This is the case for the states of Victoria (VIC) and New South Wales (NSW) and for the MDB region (Fig. 1). In fact, the variability of rainfall and $PAR_{D10}$ for VIC (the central part of SEA) is essentially the same as for SEA with CS rainfall ($PAR_{D10}$) correlation of 0.97 (0.94). Indeed, the relationships between explosive storms and SEA rainfall established in OF21 apply equally to VIC rainfall.

The Tasmanian variability of CS rainfall and $PAR_{D10}$ are less representative of SEA with correlations of 0.64 and 0.60 respectively. Interestingly, the changes in TAS rainfall and $PAR_{D10}$ have some similarities to those for SWWA in that the noteworthy reductions of total and extreme CS rainfall also commenced in the late 1970s as shown in Fig. 7 and in Table 7. However, the Tasmanian rainfall reductions have been more typical of SEA than the larger deficits for SWWA. The reductions in CS rainfall, and extreme rainfall, over the state of South Australia (SA) (not shown) have some similarities with those over SWWA (although not as large) and Tasmania in that they became evident in the late 1970s with further reductions at the start of the 21st century.

For CS total and decile 10 rainfall averages over the Southern Australian (SNA) and Eastern Australian (EA) regions (Fig. 1) the reductions became most evident at the start of the 21st century (not shown); this is also the case for the state of Queensland (QLD) and to a lesser extent even for the Northern Australian (NA) region (not shown).

https://doi.org/10.5194/wcd-2021-72
Preprint. Discussion started: 15 November 2021


In this study we shall not make an extensive analysis of the associated changes in streamflow that occurred in SEA or other regions. As might be expected from the relative changes in rainfall between SEA and SWWA the streamflow reductions into some drainage divisions across SEA have been notable but less impactful than those into Perth dams as discussed, for example, in Bureau of Meteorology and CSIRO (2020).

### 4.2 SH atmospheric circulation

The dynamical study of FF11 noted that the July rainfall reductions during 1997 to 2006, in the AMD, (compared with the baseline 1949-1968 period) were associated with reductions as large as 6 $ms^{-1}$ in the strength of the SH upper tropospheric subtropical jet centred on 30S between the longitudes of 110E and 160E. Similar increases in peak jet strength near 55S were also noted. From Figure 2 of FF11, it is evident that there was also a noteworthy reduction in the baroclinicity of the SH mid-troposphere near 30S particularly in the Australian region. OF21 further discussed the changes in the SH circulation, as characterized by several local, hemispheric, and globally important predictors or indices. In particular, they found that July SEA rainfall variability was highly correlated with the 700 hPa zonal wind in the region 20S-35S, 132.5E-155E. Table 8 shows that average the correlations between SEA and Tasmanian rainfall and this 700 hPa regional zonal wind are even larger for the seven-month cool season of April to October that for July (OF21, Table 4).

## 5 Northern Australian rainfall and rainfall extremes

While Southern Australia has undergone noteworthy reductions in rainfall since the 1970s, due largely to a reduction in storminess and, particularly, in the intensity of fast-growing extratropical storms (FF05; FF07; FF11; Hope, 2006; Alexander et al., 2011; Risbey et al., 2013; Frederiksen et al., 2017; OF21), Northern Australia (Fig. 1) has seen increased precipitation (Frederiksen and Grainger, 2015; Dey et al., 2019; Bureau of Meteorology and CSIRO, 2020 and references therein). Table 6 shows the increases in total rainfall (of circa 15%) and in extreme precipitation measured by $PAR_{D10}$ (of a nearly three-fold increase) since the late 1960s. While these increases are of importance, they cannot make up for the decreases that have occurred in the population centres and food bowls of Southern Australia which are our primary concern in this study.

## 6 South west Western Australian temperature and temperature extremes

Next, we examine the changes in Australian temperatures that have occurred primarily in the latter part of the 20th century and in two decades of the 21st century. Average Australian temperatures have increased by circa 0.9°C since 1910 with increases in the temperature extremes (Trewin and Vermont, 2010; Trewin, 2013; CSIRO and Bureau of Meteorology, 2015 reviews the literature). In this Section we start with an analysis of temperatures and temperature extremes over SWWA. Figure 8 shows time series of annual maximum temperatures and annual Percentage Area with Temperatures in Decile 10 ($PAT_{D10}$) for maximum temperatures between 1911 and 2019 for SWWA. Results are presented for variability on the annual timescale as

https://doi.org/10.5194/wcd-2021-72
Preprint. Discussion started: 15 November 2021


well as for 10 year running means which again bring out the regime transitions. Despite the interannual variability maximum temperatures have increased considerably from the early 1990s and extreme maximum temperatures from the start of the 21st century. From Table 9 we see that the increase in maximum temperatures since the early 1990s is circa 0.9ºC while the average area experiencing extreme maximum temperatures has increased from a negligible percentage to 46% of SWWA since the start of the 21st century. The average trends, or gradients, of the 10-year running means of SWWA temperatures, shown in Figs. 8c and d, are presented in Table 10 for the time spans relevant to the above regimes. We note that the gradient associated with the maximum temperature increases by a factor of nearly 5 between the early and late periods shown while the trend in maximum extreme temperatures ($PAT_{D10}$) changes from negligible (1910-2001) to 4.8% $yr^{-1}$ (2002-2019). Indeed, the rate of increase of maximum temperatures and $PAT_{D10}$ for the period 2002-2019 is higher than for any of the other major geographical regions considered next for which corresponding results are also shown in Table 10.

## 7 South east Australian temperature and temperature extremes

We now turn to regime transitions of south east Australian temperatures that began near the start of the 21st century with a focus on maximum temperatures including extreme temperatures. Figure 9a shows the annual anomaly in maximum temperatures over SEA with nearly identical results for VIC (correlation of 0.99) and quite similar results for New South Wales (NSW) and the Murray Darling Basin (MDB) (not shown). The MDB is Australia's main food bowl which stretches inland between Victoria through NSW to southern Queensland (Fig. 1). We note from Fig. 9a that while there is considerable interannual variability in the graph it is evident that maximum temperatures have increased considerably in the early 21st century compared with the 20th century. This change between centuries is more dramatic when considering extreme temperatures. Figure 9b shows time series of the annual Percentage Area with Temperatures in Decile 10 ($PAT_{D10}$) for SEA maximum temperatures with again nearly identical results for VIC (correlation of 0.99). Again, Figs. 9c and 9d show the corresponding 10-year running mean results corresponding to Figs. 9a and 9b respectively. It is clear from Fig. 9 that during the circa 20 years of the early 21st century there were many occasions when extreme maximum temperatures in the decile 10 band covered large areas of SEA compared with earlier. Figure 10 shows corresponding results for changes in annual maximum temperatures over Tasmania. We note that the temperature increases started earlier than shown for the combined temperatures for SEA in Fig. 9.

The main deductions that can be made from the results in Figs. 9 and 10 are summarised in Table 9. We note that for the whole of the SEA region, and for NSW and MDB (and VIC - not shown), annual maximum temperature anomalies averaged between 1910-2001 are quite small while in the eighteen years of 2002-2019 the differences are circa 1.1ºC to 1.2ºC. For Tasmania the change is less at circa 0.7ºC. We also see that extreme maximum temperatures have become more prevalent. For the 20th century $PAT_{D10}$ for maximum temperatures is just a few percent for SEA, NSW and MDB (and VIC - not shown) but for 2002-2019 the area of extreme maximum temperature rises to between 47% and 49% for SEA, NSW, MDB and VIC and to 32%

https://doi.org/10.5194/wcd-2021-72
Preprint. Discussion started: 15 November 2021


for Tasmania. These temperature changes for SEA are quite dramatic and if continued could have major implications for the primary food bowl of the Murray Darling Basin.

The smoothed 10-year running means of the results, shown in Figs. 9c and d for SEA (respectively Figs. 10 c and d for Tasmania), aid in the visualization of the regime transitions. It is evident that maximum temperature anomalies in SEA, and in NSW and MDB, as well as maximum temperature extremes for these regions change dramatically at the start of the 21st century. Table 10 lists the averaged trends or gradients of these 10-year running means of both annual maximum temperature anomalies and temperature extremes for 1910-2001. The distinct increases in trends in the early 21st century again support the concept of a regime transition in SEA temperatures.

For annual average maximum temperatures and $PAT_{D10}$ for maximum temperatures averages over the Southern Australian (SNA) and Eastern Australian (EA) regions (Fig. 1), and for the state of QLD, the notable increases again occurred at the start of the 21st century (not shown). For the Northern Australian (NA) region the increases in maximum temperatures and $PAT_{D10}$ started in the 1990s and became more evident during the 21st century (not shown).

## 8 Australian temperature and temperature extremes

The regime transitions of SWWA and SEA maximum temperatures and particularly extreme maximum temperatures in fact apply to extreme temperatures averaged more generally across the whole of Australia, as might be expected from the results in the previous sections. For both mean and maximum temperatures extremes characterized by $PAT_{D10}$ increase dramatically in the first two decades of the 21st century; $PAT_{D10}$ increases from just a few percent to 44% for mean and 47% for maximum temperatures for 2002-2019 as show in Table 9. Again, Table 10 shows that there is a considerable change in the averaged gradient around 2002 based on 10-year running means of $PAT_{D10}$ for both mean and maximum temperatures. The distinct increases in trends in the early 21st century again support the concept of a regime transition in Australian temperatures.

## 9 Discussion and conclusions

The main purpose of this study has been to present evidence of regime transitions during the 20th and early 21st century in important aspects of Australian climate. We have focussed on the changes over Southern Australia in rainfall, temperatures and extremes, and associated circulation features since the early 20th century. We have also examined some particularly dramatic shifts in streamflow into Perth dams.

We have found very clear signals that the climate of south-west Western Australia (SWWA) has transited into a drier and warmer state with some of these changes in rainfall, rainfall extremes and streamflow into Perth dams starting as early as the 1960s. Annual streamflow into Perth dams over the last decade has reduced to just 20% of the pre-1960s average. We have determined that the gradient of the 10-year running mean (RM) of streamflow is negligible for the period 1911-1958 followed by a steep decline between 1959 and 1978 and a lesser decline between 1979 and 2018 (circa 40% of that for 1959-1978).

https://doi.org/10.5194/wcd-2021-72
Preprint. Discussion started: 15 November 2021


Similarly, the Southern Wet Season (SWS) Percentage Area with Rainfall in Decile 10 ($PAR_{D10}$) for SWWA decreased from 16% for the period 1900-1958 to just 0.2% for 2009-2018. As in the case of streamflow into Perth dams most of the decrease in $PAR_{D10}$ occurred between 1959-1978 but with little further systematic decrease between 1979-2018. The changes in magnitude and gradients for streamflow and $PAR_{D10}$ are strong indicators of regime transitions in these variables for SWWA. Perth streamflow has been shown to be essentially proportional to the square of rainfall and is thus a more sensitive indicator than rainfall itself. Indeed, in comparison SWWA rainfall in the SWS in 2009-2018 was reduced by 21% compared with the long-term average over 1900-1958. The gradients for the 10-year RM of rainfall again show similar behaviour to Perth streamflow with the steepest drop between 1959-1978 and a lesser drop between 1959-2018 (circa 45% of that for 1959-1978). As proposed in FF07, and further established in the data driven study of OF21 for winter, reductions in the intensity of fast-growing storms in the SWWA region are responsible for the declines in rainfall. We have shown here that the atmospheric flow fields are consistent with a regime transition into a weaker zonal flow and baroclinicity state in the regions upstream and over SWWA in the twenty-year period 1959-1978.

Surface temperatures in SWWA have also increased with most of the rise occurring from the late 20$^{th}$ or early 21$^{st}$ century. Annual maximum temperatures have increased over the last 20 to 30 years by circa 0.9$^{o}$C compared with the earlier period starting in 1910. The change in extreme maximum temperatures has been more dramatic; the Percentage Area with temperatures in Decile 10 ($PAT_{D10}$) increased from 2.7% for 1910-2001 to 46% for 2002-2019. On average, maximum temperatures also increased nearly 5 times faster in 2002-2019 compared with 1910-2001 based on changes in the gradient of the 10-year RM. For $PAT_{D10}$ the average gradient was negligible for 1910-2001 but with a rapid rise of 4.8% yr$^{-1}$ for 2002-2019. These shifts in maximum temperatures (with somewhat similar shifts in mean and minimum temperatures) and extremes and their gradients are consistent with phase transitions in the temperatures of SWWA in addition to the earlier transitions in rainfall. Interestingly, the alignment of increasing areas of SWWA (Figs. 8b and d) to experiencing extreme temperatures since 2002 is reminiscent of the alignment of atomic spins in ferromagnets in transition to the magnetic state.

SWWA has seen the earliest and most dramatic systematic shifts in climate to a drier state with South-Eastern Australia (SEA) impacted towards the end of the 20$^{th}$ century. Cool Season (CS) rainfall over SEA reduced by an average of 12% between the two periods 1900-1998 and 1999-2019 while $PAR_{D10}$ reduced from 11% to 5%. For Victoria (VIC), which is the central region of SEA, the relative changes are virtually identical, and they are also very similar for New South Wales (NSW) and the Murray Darling Basin (MDB). In Tasmania (TAS), the southern part of SEA, rainfall reductions, particular for extreme rainfall, occurred earlier with $PAR_{D10}$ reducing from 12.5% to 5% between the period 1910-1978 and 1979-2019. Again, the changes in rainfall in SEA is associated with changes in the circulation over and around this region.

Annual maximum temperatures anomalies for SEA, and for VIC, NSW and MDB, averaged over the early period 1910-2001 are quite small while in the eighteen years of 2002-2019 the differences are circa 1.1$^{o}$C to 1.2$^{o}$C. For Tasmania the change is less at circa 0.7$^{o}$C. Further, $PAT_{D10}$ for SEA increased from 2.7% for 1910-2001 to 47% for 2002-2019, which is very similar to the case for SWWA and VIC, with slightly larger changes for NSW and MDB, and smaller changes for TAS. For SEA,

https://doi.org/10.5194/wcd-2021-72
Preprint. Discussion started: 15 November 2021


maximum temperatures rose circa 7 times faster in 2002-2019 compared with 1910-2001 based on changes in the gradient of the 10-yr RM. For $PAT_{D10}$ the average gradient was negligible for 1910-2001 but with a rise of 2.7% $yr^{-1}$ for 2002-2019. The regime transitions of SWWA and SEA temperatures are in fact mirrored by shifts over Australia, as a whole. This is seen particularly in extremes, with $PAT_{D10}$ increasing from very low values to 44% for mean and 47% for maximum temperatures for 2002-2019.

We note that there is considerable interannual variability in average and extreme rainfall and temperatures and in streamflow into Perth dams. For that reason, we have also examined 10-year running means to see the systematic changes in the climate variables and their gradients. We have noted discontinuities in the average gradients of the smoothed data typical of second order regime transitions. However, the large and sudden shifts in the temperature extremes are suggestive of first order regime transitions.

*Code availability*. Reasonable requests for access to code used to generate the results in the paper will be considered by contacting the authors.

*Data availability*. Atmospheric circulation data is available from the NOAA/ESRL web site: http://www.esrl.noaa.gov/psd/ and rainfall and temperature data is available form the Australian Bureau of Meteorology web site: http://www.bom.gov.au/climate/change/index.shtml#tabs=Tracker&tracker=timeseries&tQ=graph%3Drain%26area%3Daus%26season%3Dallmonths%26ave_yr%3D0

The data for streamflow into Perth dams is available from the Western Australian Water Corporation web site: https://www.watercorporation.com.au/Our-water/Rainfall-and-dams/Streamflow

*Author contributions.* J. S. Frederiksen conceived and designed the analysis, wrote the original draft, reviewed and edited, performed data analysis, supervised and mentored, and S. L. Osbrough contributed to writing, reviewing and editing, developed code, developed graphics for visualisation, and contributed to analysis, validation and reproducibility of results.

*Competing interests.* The authors declare that they have no conflicts of interest.

*Acknowledgements.* This work was supported by the Australian Government's Australian Climate Service and the Australian Research Council Centre of Excellence for Climate Extremes. Stacey L. Osbrough is an employee of the Commonwealth Scientific and Industrial Research Organisation and concurrently a Ph.D. student at Monash University to which this work contributes. Jorgen S. Frederiksen is an honorary fellow at Commonwealth Scientific and Industrial Research Organisation and Professor of Research at Monash University and is independently self-funded.

https://doi.org/10.5194/wcd-2021-72
Preprint. Discussion started: 15 November 2021


## References

Alexander, L. V. and Arblaster, J. M.: Historical and projected trends in temperature and precipitation extremes in Australia in observations and CMIP5, Weather Clim Extreme, 15, 34-56, https://doi.org/10.1016/j.wace.2017.02.001, 2017.

Alexander, L. V., Wang, X. L. L., Wan, H., and Trewin, B.: Significant decline in storminess over southeast Australia since the late 19th century, Aust Meteorol Ocean, 61, 23-30, 10.22499/2.6101.002, 2011.

Australian Academy of Science: The risks to Australia of a 3°C warmer world, 2021.

Ball, R.: Distilled turbulence:: A reduced model for confinement transitions in magnetic fusion plasmas in: World Sci Lect Notes, 395-414, 10.1142/9789812771025_0016, 2007.

Bates, B. C., Hope, P., Ryan, B., Smith, I., and Charles, S.: Key findings from the Indian Ocean Climate Initiative and their impact on policy development in Australia, Climatic Change, 89, 339-354, 10.1007/s10584-007-9390-9, 2008.

Budyko, M. I.: The effect of solar radiation variations on the climate of the Earth, Tellus, 21, 611-619, 10.3402/tellusa.v21i5.10109, 1969.

Bureau of Meteorology: Australian climate variability and change - Time series graphs: http://www.bom.gov.au/climate/change/index.shtml#tabs=Tracker&tracker=timeseries, last access: 14/09/2021.

Bureau of Meteorology and CSIRO: State of the Climate 2020: www.csiro.au/state-of-the-climate, last access: 15/10/2021.

Cai, W., Cowan, T., and Sullivan, A.: Recent unprecedented skewness towards positive Indian Ocean Dipole occurrences and its impact on Australian rainfall, Geophys Res Lett, 36, L11705, 10.1029/2009gl037604, 2009.

Cai, W., Purich, A., Cowan, T., van Rensch, P., and Weller, E.: Did Climate Change–Induced Rainfall Trends Contribute to the Australian Millennium Drought?, J Climate, 27, 3145-3168, 10.1175/jcli-d-13-00322.1, 2014.

Charney, J. G. and Devore, J. G.: Multiple Flow Equilibria in the Atmosphere and Blocking, J Atmos Sci, 36, 1205-1216, 10.1175/1520-0469(1979)036<1205:Mfeita>2.0.Co;2, 1979.

Charney, J. G. and Straus, D. M.: Form-drag instability, multiple equilibria and propagating planetary waves in baroclinic, orographically forced, planetary wave systems, Journal of Atmospheric Sciences, 37, 1157-1176, https://doi.org/10.1175/1520-0469(1980)037<1157:FDIMEA>2.0.CO;2, 1980.

Corti, S., Molteni, F., and Palmer, T. N.: Signature of recent climate change in frequencies of natural atmospheric circulation regimes, Nature, 398, 799-802, 10.1038/19745, 1999.

CSIRO and Bureau of Meteorology: Climate Change in Australia: Projections for Australia's NRM regions., CSIRO and Bureau of Meterology, Australia, Technical Report, 222, 2015.

Dey, R., Lewis, S., Abram, N., and Arblaster, J.: A review of past and projected changes in Australia's rainfall, Wiley Interdisciplinary Reviews: Climate Change, 10.1002/wcc.577, 2019.

Dijkstra, H. A.: Nonlinear Climate Dynamics, Cambridge University Press, Cambridge, 10.1017/CBO9781139034135, 2013.

Dijkstra, H. A.: Numerical bifurcation methods applied to climate models: analysis beyond simulation, Nonlinear Proc Geoph, 26, 359-369, 10.5194/npg-26-359-2019, 2019.

Fabiano, F., Meccia, V. L., Davini, P., Ghinassi, P., and Corti, S.: A regime view of future atmospheric circulation changes in northern mid-latitudes, Weather and Climate Dynamics, 2, 163-180, 10.5194/wcd-2-163-2021, 2021.

Faegre, A.: An Intransitive Model of the Earth-Atmosphere-Ocean System, J Appl Meteorol Clim, 11, 4-6, 10.1175/1520-0450(1972)011<0004:Aimote>2.0.Co;2, 1972.

Fawcett, R. J. B.: Seasonal climate summary southern hemisphere (summer 2003/04): a warm summer in the east and wet conditions in the northwest, Aust Meteorol Mag, 53, 305-317, 2004.

Franzke, C. L. E., O'Kane, T. J., Monselesan, D. P., Risbey, J. S., and Horenko, I.: Systematic attribution of observed Southern Hemisphere circulation trends to external forcing and internal variability, Nonlinear Proc Geoph, 22, 513-525, 10.5194/npg-22-513-2015, 2015.

Frederiksen, C. S. and Frederiksen, J. S.: Flow over Topography and Instability on Beta-Planes - the Effects of Different Expansion Representations, J Atmos Sci, 46, 1664-1686, 10.1175/1520-0469(1989)046<1664:Fotaio>2.0.Co;2, 1989.

Frederiksen, C. S. and Grainger, S.: The role of external forcing in prolonged trends in Australian rainfall, Clim Dynam, 45, 2455-2468, 10.1007/s00382-015-2482-8, 2015.

Frederiksen, C. S., Frederiksen, J. S., Sisson, J. M., and Osbrough, S. L.: Trends and projections of Southern Hemisphere baroclinicity: the role of external forcing and impact on Australian rainfall, Clim Dynam, 48, 3261-3282, 10.1007/s00382-016-3263-8, 2017.

https://doi.org/10.5194/wcd-2021-72
Preprint. Discussion started: 15 November 2021


Frederiksen, J. S.: Nonlinear albedo-temperature coupling in climate models, Journal of Atmospheric Sciences, 33, 2267-2272, 1976.
Frederiksen, J. S.: Instability of planetary waves and zonal flows in two-layer models on a sphere, Q J Roy Meteor Soc, 104, 841-872, 10.1002/qj.49710444202, 1978.
Frederiksen, J. S.: Strongly nonlinear topographic instability and phase transitions, Geophys Astro Fluid, 32, 103-122, 10.1080/03091928508208780, 1985.
Frederiksen, J. S.: Nonlinear Studies on the Effects of Topography on Baroclinic Zonal Flows, Geophys Astro Fluid, 59, 57-82, 1991.
Frederiksen, J. S.: Quasi-diagonal inhomogeneous closure for classical and quantum statistical dynamics, J Math Phys, 58, 10.1063/1.5006938, 2017.
Frederiksen, J. S. and Francey, R. J.: Unprecedented strength of Hadley circulation in 2015-2016 impacts on CO2 interhemispheric difference, Atmos Chem Phys, 18, 14837-14850, 10.5194/acp-18-14837-2018, 2018.
Frederiksen, J. S. and Frederiksen, C. S.: Decadal changes in Southern Hemisphere winter cyclogenesis, CSIRO Marine and Atmospheric research paper, 002, 29, http://www.cmar.csiro.au/e-print/open/frederiksenjs_2005b.pdf, 2005.
Frederiksen, J. S. and Frederiksen, C. S.: Interdecadal changes in southern hemisphere winter storm track modes, Tellus A, 59, 599-617, 10.1111/j.1600-0870.2007.00264.x, 2007.
Frederiksen, J. S. and Frederiksen, C. S.: Twentieth Century Winter Changes in Southern Hemisphere Synoptic Weather Modes, Adv Meteorol, 2011, 10.1155/2011/353829, 2011.
Frederiksen, J. S., Collier, M. A., and Watkins, A. B.: Ensemble prediction of blocking regime transitions, Tellus A, 56, 485-500, DOI 10.1111/j.1600-0870.2004.00075.x, 2004.
Frederiksen, J. S., Frederiksen, C. S., Osbrough, S. L., and Sisson, J. M.: Causes of changing Southern Hemisphere weather systems, Managing Climate Change, 8, 85-98, 2010.
Freitas, A. C. V., Frederiksen, J. S., Whelan, J., O'Kane, T. J., and Ambrizzi, T.: Observed and simulated inter-decadal changes in the structure of Southern Hemisphere large-scale circulation, Clim Dynam, 45, 2993-3017, 10.1007/s00382-015-2519-z, 2015.
Gallant, A. J. E., Hennessy, K. J., and Risbey, J.: Trends in rainfall indices for six Australian regions: 1910-2005, Aust Meteorol Mag, 56, 223-239, 2007.
Ghil, M.: Climate Stability for a Sellers-Type Model, J Atmos Sci, 33, 3-20, 10.1175/1520-0469(1976)033<0003:Csfast>2.0.Co;2, 1976.
Grose, M. R., Foster, S., Risbey, J. S., Osbrough, S., and Wilson, L.: Using indices of atmospheric circulation to refine southern Australian winter rainfall climate projections, Clim Dynam, 53, 5481-5493, 10.1007/s00382-019-04880-4, 2019.
Harter, J. W., Zhao, Z. Y., Yan, J. Q., Mandrus, D. G., and Hsieh, D.: A parity-breaking electronic nematic phase transition in the spin-orbit coupled metal Cd2Re2O7, Science, 356, 295-297, 10.1126/science.aad1188, 2017.
Hope, P. K.: Projected future changes in synoptic systems influencing southwest Western Australia, Clim Dynam, 26, 765-780, 10.1007/s00382-006-0116-x, 2006.
Jones, D. A., Wang, W., and Fawcett, R.: High-quality spatial climate data-sets for Australia, Aust Meteorol Ocean, 58, 233-248, 10.22499/2.5804.003, 2009.
Jones, R. N. and Ricketts, J. H.: Reconciling the signal and noise of atmospheric warming on decadal timescales, Earth Syst. Dynam., 8, 177-210, 10.5194/esd-8-177-2017, 2017.
Kalnay, E., Kanamitsu, M., Kistler, R., Collins, W., Deaven, D., Gandin, L., Iredell, M., Saha, S., White, G., Woollen, J., Zhu, Y., Chelliah, M., Ebisuzaki, W., Higgins, W., Janowiak, J., Mo, K. C., Ropelewski, C., Wang, J., Leetmaa, A., Reynolds, R., Jenne, R., and Joseph, D.: The NCEP/NCAR 40-year reanalysis project, Bulletin of the American Meteorological Society, 77, 437-471, 10.1175/1520-0477(1996)077<0437:TNYRP>2.0.CO;2, 1996.
Kypke, K. L., Langford, W. F., and Willms, A. R.: Anthropocene climate bifurcation, Nonlin. Processes Geophys., 27, 391-409, 10.5194/npg-27-391-2020, 2020.
L'Heureux, M. L., Takahashi, K., Watkins, A. B., Barnston, A. G., Becker, E. J., Di Liberto, T. E., Gamble, F., Gottschalck, J., Halpert, M. S., and Huang, B.: Observing and predicting the 2015/16 El Niño, Bulletin of the American Meteorological Society, 98, 1363-1382, 2017.
Lenton, T. M. R., J.; Gaffney, O.; Rahmstorf, S.; Richardson, K.; Steffen, W.; Schellnhuber, H. J. : Climate tipping points — too risky to bet against, Nature, 575, 592 - 595, 2019.

https://doi.org/10.5194/wcd-2021-72
Preprint. Discussion started: 15 November 2021


McComb, D.: Renormalization Methods: A Guide for Beginners, 58, 62-63, 10.1063/1.1996480, 2004.
O'Kane, T. J., Risbey, J. S., Franzke, C., Horenko, I., and Monselesan, D. P.: Changes in the Metastability of the Midlatitude Southern Hemisphere Circulation and the Utility of Nonstationary Cluster Analysis and Split-Flow Blocking Indices as Diagnostic Tools, J Atmos Sci, 70, 824-842, 10.1175/JAS-D-12-028.1, 2013.
Osbrough, S. L. and Frederiksen, J. S.: Interdecadal changes in Southern Hemisphere winter explosive storms and Southern Australian rainfall, Clim Dynam, 56, 3103-3130, 10.1007/s00382-021-05633-y, 2021.
Patashinski, A. and Pokrovskii, V.: Fluctuation theory of phase transitions, Pergamon Press1979.
Pezza, A. B., Durrant, T., Simmonds, I., and Smith, I.: Southern Hemisphere Synoptic Behavior in Extreme Phases of SAM, ENSO, Sea Ice Extent, and Southern Australia Rainfall, J Climate, 21, 5566-5584, 10.1175/2008jcli2128.1, 2008.
Pittock, A.: Actual and anticipated changes in Australia's climate, Greenhouse: planning for climate change, 35-51, 1988.
Pook, M. J., Risbey, J. S., and McIntosh, P. C.: The Synoptic Climatology of Cool-Season Rainfall in the Central Wheatbelt of Western Australia, Mon Weather Rev, 140, 28-43, 10.1175/Mwr-D-11-00048.1, 2012.
Quinting, J. F., Catto, J. L., and Reeder, M. J.: Synoptic climatology of hybrid cyclones in the Australian region, Q J Roy Meteor Soc, 145, 288-302, 10.1002/qj.3431, 2019.
Risbey, J. S., McIntosh, P. C., and Pook, M. J.: Synoptic components of rainfall variability and trends in southeast Australia, Int J Climatol, 33, 2459-2472, 10.1002/joc.3597, 2013.
Sadler, B., Mauger, G., and Stokes, R.: The water resource implications of a drying climate in south-west Western Australia, Greenhouse: Planning for Climate Change, CSIRO, Melbourne, 296-311, 1988.
Saghayezhian, M., Kouser, S., Wang, Z., Guo, H. W., Jin, R. Y., Zhang, J. D., Zhu, Y. M., Pantelides, S. T., and Plummer, E. W.: Atomic-scale determination of spontaneous magnetic reversal in oxide heterostructures, P Natl Acad Sci USA, 116, 10309-10316, 10.1073/pnas.1819570116, 2019.
Schneider, S. and Gal-Chen, T.: Numerical experiments in climate stability, J Geophys Res, 78, 6182-6194, 1973.
Sellers, W. D.: A Global Climatic Model Based on the Energy Balance of the Earth-Atmosphere System, J Appl Meteorol Clim, 8, 392-400, 10.1175/1520-0450(1969)008<0392:Agcmbo>2.0.Co;2, 1969.
Thompson, C. J.: Mathematical Statistical Mechanics, Princeton University Press, 290 pp., 10.1515/9781400868681, 1979.
Trewin, B.: A daily homogenized temperature data set for Australia, Int J Climatol, 33, 1510-1529, 10.1002/joc.3530, 2013.
Trewin, B. and Vermont, H.: Changes in the frequency of record temperature in Australia, 1957-2009, Aust. Meteorol. Oceanogr. J, 60, 10.22499/2.6002.003, 2010.
Water Corporation: Water Corporation https://pw-cdn.watercorporation.com.au/Our-water/Rainfall-and-dams/Streamflow, last access: 14/08/2020.
Watkins, A. and Trewin, B.: Australian climate summary: 2006, Bulletin of the Australian Meteorological and Oceanographic Society, 20, 10-17, 2007.
Whelan, J. A. and Frederiksen, J. S.: Dynamics of the perfect storms: La Niña and Australia's extreme rainfall and floods of 1974 and 2011, Clim Dynam, 48, 3935-3948, 2017.
Wiin-Nielsen, A.: Steady states and stability properties of a low-order barotropic system with forcing and dissipation, Tellus, 31, 375-386, 10.3402/tellusa.v31i5.10452, 1979.
Wilson, K. G.: Problems in Physics with many Scales of Length, Sci Am, 241, 158-179, 10.1038/scientificamerican0879-158, 1979.
Wilson, K. G. and Kogut, J.: The renormalization group and the ϵ expansion, Physics Reports, 12, 75-199, 10.1016/0370-1573(74)90023-4, 1974.
Yan, P., Feng, G., Hou, W., and Yang, P.: A method for predicting the uncompleted climate transition process, Nonlin. Processes Geophys., 27, 489-500, 10.5194/npg-27-489-2020, 2020.
Zidikheri, M. J., Frederiksen, J. S., and O'Kane, T. J.: Multiple equilibria and atmospheric blocking., in: World Sci Lect Notes, 59-85, 10.1142/9789812771025_0003, 2007.

https://doi.org/10.5194/wcd-2021-72
Preprint. Discussion started: 15 November 2021


**Table captions**

Table 1: The mean SWWA rainfall in SWS, January to December streamflow into Perth dams and percentage area of SWWA with SWS rainfall in decile 10 (PARD10) for different time periods.

Table 2: Correlations $(r)$ between SWWA rainfall, PARD10, streamflow into Perth dams (as in Table 1), rainfall squared and a quadratic fit of rainfall to streamflow with detrended correlations in brackets.

Table 3: The average gradients or trends of 10-year RM of SWWA rainfall in SWS, January to December streamflow into Perth dams and percentage area of SWWA with SWS rainfall in decile 10 (PARD10) for different time periods.

Table 4: The mean April-November (SWS) 150 hPa zonal wind averaged between 30° S – 35 ° S, 100° E – 130° E, 300 hPa minus 700 hPa zonal wind shear averaged between 30° S – 35 ° S, 100° E – 130° E and 700 hPa zonal wind averaged between 20° S – 35 ° S, 110° E – 132.5° E, for different time periods.

Table 5: The average gradients or trends of SWS 150 hPa zonal wind averaged between 30° S – 35 ° S, 100° E – 130° E, 300 hPa minus 700 hPa zonal wind shear averaged between 30° S – 35 ° S, 100° E – 130° E and 700 hPa zonal wind averaged between 20° S – 35 ° S, 110° E – 132.5° E, for different time periods.

Table 6: Correlations $(r)$, and detrended correlations in brackets, of SWWA rainfall, PARD10, streamflow into Perth dams, rainfall squared and a quadratic fit of rainfall to streamflow with SWS 300 hPa minus 700 hPa zonal wind shear averaged between 30° S – 35 ° S, 100° E – 130° E and 700 hPa zonal wind averaged between 20° S – 35 ° S, 110° E – 132.5° E.

Table 7: As in Table 1 for SEA and TAS Cool Season (CS) rainfall and PARD10 and NA Northern Wet Season (NWS) rainfall and PARD10.

Table 8: Correlations $(r)$, and detrended correlations in brackets, of SEA and TAS Cool Season (CS) and Southern Wet Season (SWS) rainfall with 700 hPa zonal wind averaged between 20° S – 35 ° S, 132.5° E – 155° E.

Table 9: The annual mean of maximum temperatures and percentage areas with maximum temperatures in decile 10 (PATD10) for SWWA, SEA, NSW, MDB and TAS and Australian PATD10 for mean and maximum temperatures, for different time periods.

Table 10: As in Table 9 for the gradients or trends of 10-year RM of the temperatures and PATD10.

**Figure captions**

Figure 1: Map of Australian regions showing South-western (SWWA), South-eastern (SEA – with a box around Tasmania), Eastern (EA), Southern (SNA), Northern (NA) and Murray Darling Basin (MBD) areas for averaged rainfall and temperature data.

Figure 2: Interannual variability of (a) SWWA rainfall totals (mm) for April-November (SWS), (b) percentage area (%) of SWWA with rainfall in decile 10 (PARD10) for SWS and (c) January-December streamflow (GL) into Perth dams.

Figure 3: As in Figure 2 for 10-year running means (RM) of rainfall and streamflow data.

https://doi.org/10.5194/wcd-2021-72
Preprint. Discussion started: 15 November 2021




Figure 4: Vertical cross-section of April-November zonal wind (m $s^{-1}$) averaged between 100° E – 130° E as a function of latitude and pressure (p in hPa) for (1975–1994) minus (1949–1968). Contour intervals are 1 $ms^{-1}$.

Figure 5: Interannual variability of April-November (a) 150 hPa zonal wind averaged between 30° S – 35° S, 100° E – 130° E and (b) 300 hPa minus 700 hPa zonal wind shear averaged between 30° S – 35° S, 100° E – 130° E.

Figure 6: (a) SEA rainfall totals (mm) for April-October (CS), (b) percentage area (%) of SEA with rainfall in decile 10 (PARD10) for CS (c) 10-year RM of SEA rainfall totals for CS and (d) 10-year RM of SEA PARD10 for CS.

Figure 7: As in Figure 6 for TAS.

Figure 8: (a) SWWA annual maximum temperature variability (°C), (b) SWWA percentage area (%) with maximum annual temperatures in decile 10 (PATD10), (c) 10-year RM of SWWA annual maximum temperatures and (d) 10-year RM of SWWA PATD10.

Figure 9: As in Figure 8 for SEA.

Figure 10: As in Figure 8 for TAS.

https://doi.org/10.5194/wcd-2021-72
Preprint. Discussion started: 15 November 2021


**Tables**

Table 1

| Time Period | Variable | Mean |
|---|---|---|
| 1900-1958 | SWWA Rainfall SWS | 639 mm $yr^{-1}$ |
| 1959-1978 | SWWA Rainfall SWS | 610 mm $yr^{-1}$ |
| 1979-2018 | SWWA Rainfall SWS | 545 mm $yr^{-1}$ |
| 2009-2018 | SWWA Rainfall SWS | 502 mm $yr^{-1}$ |
| 2014-2018 | SWWA Rainfall SWS | 500 mm $yr^{-1}$ |
| 1911-1958 | Perth Streamflow | 414 gl $yr^{-1}$ |
| 1959-1978 | Perth Streamflow | 389 gl $yr^{-1}$ |
| 1979-2018 | Perth Streamflow | 183 gl $yr^{-1}$ |
| 2009-2018 | Perth Streamflow | 88 gl $yr^{-1}$ |
| 2014-2018 | Perth Streamflow | 76 gl $yr^{-1}$ |
| 1900-1958 | SWWA % Area- Rainfall Decile 10 SWS | 15.5% |
| 1959-1978 | SWWA % Area- Rainfall Decile 10 SWS | 10.3% |
| 1979-2018 | SWWA % Area-Rainfall Decile 10 SWS | 2.03% |
| 2009-2018 | SWWA % Area-Rainfall Decile 10 SWS | 0.19% |
| 2014-2018 | SWWA % Area-Rainfall Decile 10 SWS | 0.38% |

575

Table 2

| | Rainfall SWS | Streamflow |
|---|---|---|
| Rainfall SWS | $r$ = 1.0 (1.0) | $r$ = 0.84 (0.81) |
| Streamflow Jan-Dec | $r$ = 0.84 (0.81) | $r$ = 1.0 (1.0) |
| Percentage Area Rainfall Decile 10 | $r$ = 0.74 (0.73) | $r$ = 0.79 (0.78) |
| Rainfall Squared | $r$ = 0.99 (0.90) | $r$ = 0.87 (0.84) |
| Quadratic Fit | $r$ = 0.96 (0.95) | $r$ = 0.88 (0.86) |

https://doi.org/10.5194/wcd-2021-72
Preprint. Discussion started: 15 November 2021


Table 3

| Time Period | Variable | Gradient |
|---|---|---|
| 1900-1958 | SWWA Rainfall SWS 10yr RM | -0.81 mm $yr^{-2}$ |
| 1959-1978 | SWWA Rainfall SWS 10yr RM | -4.0 mm $yr^{-2}$ |
| 1979-2018 | SWWA Rainfall SWS 10yr RM | -1.8 mm $yr^{-2}$ |
| 1911-1958 | Perth Streamflow 10yr RM | 0.20 gl $yr^{-2}$ |
| 1959-1978 | Perth Streamflow 10yr RM | -11.1 gl $yr^{-2}$ |
| 1979-2018 | Perth Streamflow 10yr RM | -5.4 gl $yr^{-2}$ |
| 1900-1958 | SWWA % Area- Rainfall Decile 10 SWS 10yr RM | -0.11 % $yr^{-1}$ |
| 1959-1978 | SWWA % Area- Rainfall Decile 10 SWS 10yr RM | -0.76 % $yr^{-1}$ |
| 1979-2018 | SWWA % Area-Rainfall Decile 10 SWS 10yr RM | -0.04 % $yr^{-1}$ |

580

Table 4

| Time Period | Variable | Mean |
|---|---|---|
| 1948-1958 | U150 30S-35S 100E-130E SWS | 42.1 $ms^{-1}$ |
| 1959-1978 | U150 30S-35S 100E-130E SWS | 37.9 $ms^{-1}$ |
| 1979-2018 | U150 30S-35S 100E-130E SWS | 34.4 $ms^{-1}$ |
| 1948-1958 | U300 – U700 30S-35S 100E-130E SWS | 24.0 $ms^{-1}$ |
| 1959-1978 | U300 – U700 30S-35S 100E-130E SWS | 21.4 $ms^{-1}$ |
| 1979-2018 | U300 – U700 30S-35S 100E-130E SWS | 20.1 $ms^{-1}$ |
| 1948-1958 | U700 20S-35S 110E-132.5E SWS | 6.76 $ms^{-1}$ |
| 1959-1978 | U700 20S-35S 110E-132.5E SWS | 6.12 $ms^{-1}$ |
| 1979-2018 | U700 20S-35S 110E-132.5E SWS | 5.92 $ms^{-1}$ |

Table 5

| Time Period | Variable | Gradient |
|---|---|---|
| 1959-1978 | U150 30S-35S 100E-130E SWS 10yr RM | -0.33 $ms^{-1}$ $yr^{-1}$ |
| 1979-2018 | U150 30S-35S 100E-130E SWS 10yr RM | -0.003 $ms^{-1}$ $yr^{-1}$ |
| 1959-1978 | U300 – U700 30S-35S 100E-130E SWS 10yr RM | -0.22 $ms^{-1}$ $yr^{-1}$ |
| 1979-2018 | U300 – U700 30S-35S 100E-130E SWS 10yr RM | -0.015 $ms^{-1}$ $yr^{-1}$ |
| 1959-1978 | U700 20S-35S 110E-132.5E SWS 10yr RM | -0.018 $ms^{-1}$ $yr^{-1}$ |
| 1979-2018 | U700 20S-35S 110E-132.5E SWS 10yr RM | -0.019 $ms^{-1}$ $yr^{-1}$ |

585

https://doi.org/10.5194/wcd-2021-72
Preprint. Discussion started: 15 November 2021


Table 6

| | U300 – U700 30S-35S 100E-130E SWS | U700 20S-35S 100E-132.5E SWS |
|---|---|---|
| Rainfall SWS | $r$ = 0.58 (0.51) | $r$ = 0.66 (0.63) |
| Streamflow Jan-Dec | $r$ = 0.56 (0.451) | $r$ = 0.57 (0.54) |
| Rainfall % Area Decile 10 | $r$ = 0.359 (0.29) | $r$ = 0.34 (0.29) |
| Rainfall Squared | $r$ = 0.58 (0.51) | $r$ = 0.64 (0.61) |
| Quadratic Fit | $r$ = 0.56 (0.49) | $r$ = 0.60 (0.57) |

Table 7

| Time Period | Variable | Mean |
|---|---|---|
| 1900-1998 | SEA Rainfall CS | 410 mm $yr^{-1}$ |
| 1999-2019 | SEA Rainfall CS | 361 mm $yr^{-1}$ |
| 1900-1998 | SEA % Area- Rainfall Decile 10 CS | 11.0% |
| 1999-2019 | SEA % Area- Rainfall Decile 10 CS | 5.15% |
| 1900-1978 | TAS Rainfall CS | 934 mm $yr^{-1}$ |
| 1979-2019 | TAS Rainfall CS | 914 mm $yr^{-1}$ |
| 1900-1978 | TAS % Area- Rainfall Decile 10 CS | 12.5% |
| 1979-2019 | TAS % Area- Rainfall Decile 10 CS | 5.15% |
| 1900-1968 | NA Rainfall NWS | 437 mm $yr^{-1}$ |
| 1969-2019 | NA Rainfall NWS | 509 mm $yr^{-1}$ |
| 1900-1968 | NA % Area- Rainfall Decile 10 NWS | 5.45% |
| 1969-2019 | NA % Area- Rainfall Decile 10 NWS | 16.2% |

590

Table 8

| | U700 20S-35S 132.5E-155E |
|---|---|
| SEA Rainfall CS | $r$ = 0.73 (0.73) |
| SEA Rainfall SWS | $r$ = 0.72 (0.73) |
| TAS Rainfall CS | $r$ = 0.75 (0.74) |
| TAS Rainfall SWS | $r$ = 0.73 (0.73) |

https://doi.org/10.5194/wcd-2021-72
Preprint. Discussion started: 15 November 2021


595

Table 9

| Time Period | Variable | Mean |
|---|---|---|
| 1910-1991 | SWWA Max Temp Anomaly Annual | -0.21ºC |
| 1992-2019 | SWWA Max Temp Anomaly Annual | 0.67ºC |
| 1910-2001 | SWWA Max Temp Anomaly Annual | -0.27ºC |
| 2002-2019 | SWWA Max Temp Anomaly Annual | 0.46ºC |
| 1910-2001 | SWWA % Area with Max Temp Decile 10 Ann | 2.7% |
| 2002-2019 | SWWA % Area with Max Temp Decile 10 Ann | 46.0% |
| 1910-2001 | SEA Max Temp Anomaly Annual | -0.11ºC |
| 2002-2019 | SEA Max Temp Anomaly Annual | 1.02ºC |
| 1910-2001 | NSW Max Temp Anomaly Annual | -0.03ºC |
| 2002-2019 | NSW Max Temp Anomaly Annual | 1.23ºC |
| 1910-2001 | MDB Max Temp Anomaly Annual | -0.02ºC |
| 2002-2019 | MDB Max Temp Anomaly Annual | 1.22ºC |
| 1910-2001 | TAS Max Temp Anomaly Annual | -0.22ºC |
| 2002-2019 | TAS Max Temp Anomaly Annual | 0.49ºC |
| 1910-2001 | SEA % Area with Max Temp Decile 10 Ann | 2.7% |
| 2002-2019 | SEA % Area with Max Temp Decile 10 Ann | 47.2% |
| 1910-2001 | NSW % Area with Max Temp Decile 10 Ann | 2.4% |
| 2002-2019 | NSW % Area with Max Temp Decile 10 Ann | 49.0% |
| 1910-2001 | MDB % Area with Max Temp Decile 10 Ann | 2.4% |
| 2002-2019 | MDB % Area with Max Temp Decile 10 Ann | 49.0% |
| 1910-2001 | TAS % Area with Max Temp Decile 10 Ann | 5.7% |
| 2002-2019 | TAS % Area with Max Temp Decile 10 Ann | 31.9% |
| 1910-2001 | AUS % Area with Mean Temp Decile 10 Ann | 3.3% |
| 2002-2019 | AUS % Area with Mean Temp Decile 10 Ann | 44.3% |
| 1910-2001 | AUS % Area with Max Temp Decile 10 Ann | 2.8% |
| 2002-2019 | AUS % Area with Max Temp Decile 10 Ann | 46.6% |

https://doi.org/10.5194/wcd-2021-72
Preprint. Discussion started: 15 November 2021


Table 10

| Time Period | Variable | Gradient |
|---|---|---|
| 1910-1991 | SWWA Max Temp Anomaly Annual 10yr RM | 0.73 x$10^{-2}$ $^{o}$C yr$^{-1}$ |
| 1992-2019 | SWWA Max Temp Anomaly Annual 10yr RM | 3.7 x$10^{-2}$ $^{o}$C yr$^{-1}$ |
| 1910-2001 | SWWA Max Temp Anomaly Annual 10yr RM | 0.93 x$10^{-2}$ $^{o}$C yr$^{-1}$ |
| 2002-2019 | SWWA Max Temp Anomaly Annual 10yr RM | 4.5 x$10^{-2}$ $^{o}$C yr$^{-1}$ |
| 1910-2001 | SWWA % Area with Max Temp Decile 10 Ann 10yr RM | 0.11 % yr$^{-1}$ |
| 2002-2019 | SWWA % Area with Max Temp Decile 10 Ann 10yr RM | 4.8 % yr$^{-1}$ |
| 1910-2001 | SEA Max Temp Anomaly Annual 10yr RM | 0.45 x$10^{-2}$ $^{o}$C yr$^{-1}$ |
| 2002-2019 | SEA Max Temp Anomaly Annual 10yr RM | 3.00 x$10^{-2}$ $^{o}$C yr$^{-1}$ |
| 1910-2001 | NSW Max Temp Anomaly Annual 10yr RM | 0.36 x$10^{-2}$ $^{o}$C yr$^{-1}$ |
| 2002-2019 | NSW Max Temp Anomaly Annual 10yr RM | 3.5 x$10^{-2}$ $^{o}$C yr$^{-1}$ |
| 1910-2001 | MDB Max Temp Anomaly Annual 10yr RM | 0.33 x$10^{-2}$ $^{o}$C yr$^{-1}$ |
| 2002-2019 | MDB Max Temp Anomaly Annual 10yr RM | 3.2 x$10^{-2}$ $^{o}$C yr$^{-1}$ |
| 1910-2001 | TAS Max Temp Anomaly Annual 10yr RM | 0.73 x$10^{-2}$ $^{o}$C yr$^{-1}$ |
| 2002-2019 | TAS Max Temp Anomaly Annual 10yr RM | 1.9 x$10^{-2}$ $^{o}$C yr$^{-1}$ |
| 1910-2001 | SEA % Area with Max Temp Decile 10 Ann 10yr RM | 0.002% yr$^{-1}$ |
| 2002-2019 | SEA % Area with Max Temp Decile 10 Ann 10yr RM | 2.7 % yr$^{-1}$ |
| 1910-2001 | NSW % Area with Max Temp Decile 10 Ann 10yr RM | 0.0002 % yr$^{-1}$ |
| 2002-2019 | NSW % Area with Max Temp Decile 10 Ann 10yr RM | 2.2 % yr$^{-1}$ |
| 1910-2001 | MDB % Area with Max Temp Decile 10 Ann 10yr RM | -0.02 % yr$^{-1}$ |
| 2002-2019 | MDB % Area with Max Temp Decile 10 Ann 10yr RM | 2.2 % yr$^{-1}$ |
| 1910-2001 | TAS % Area with Max Temp Decile 10 Ann 10yr RM | 0.02 % yr$^{-1}$ |
| 2002-2019 | TAS % Area with Max Temp Decile 10 Ann 10yr RM | 2.0 % yr$^{-1}$ |
| 1910-2001 | AUS % Area with Mean Temp Decile 10 Ann 10yr RM | 0.14 % yr$^{-1}$ |
| 2002-2019 | AUS % Area with Mean Temp Decile 10 Ann 10yr RM | 2.9 % yr$^{-1}$ |
| 1910-2001 | AUS % Area with Max Temp Decile 10 Ann 10yr RM | 0.05 % yr$^{-1}$ |
| 2002-2019 | AUS % Area with Max Temp Decile 10 Ann 10yr RM | 2.5 % yr$^{-1}$ |

600

https://doi.org/10.5194/wcd-2021-72
Preprint. Discussion started: 15 November 2021


**Figures**

Figure 1

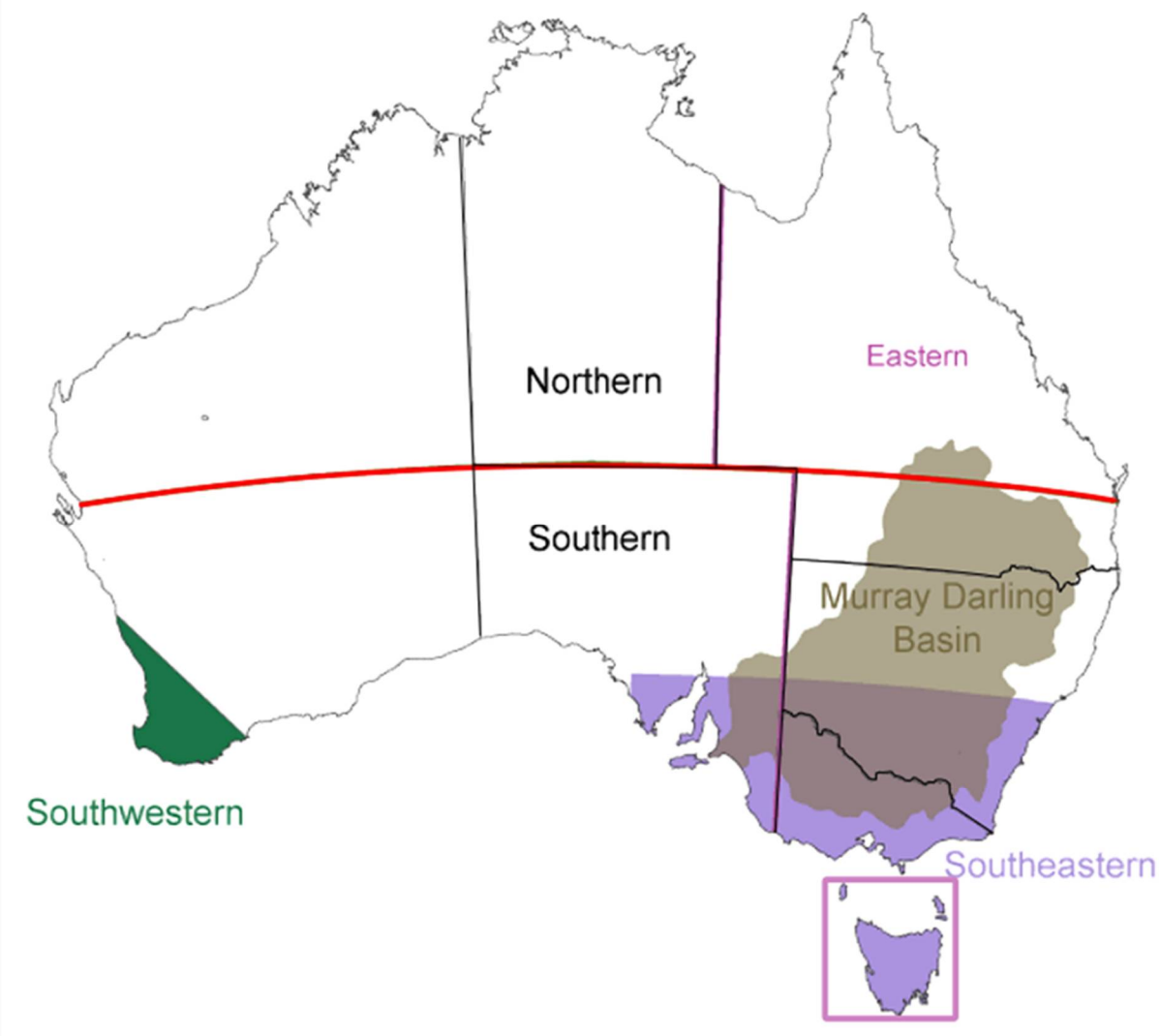

https://doi.org/10.5194/wcd-2021-72
Preprint. Discussion started: 15 November 2021


Figure 2

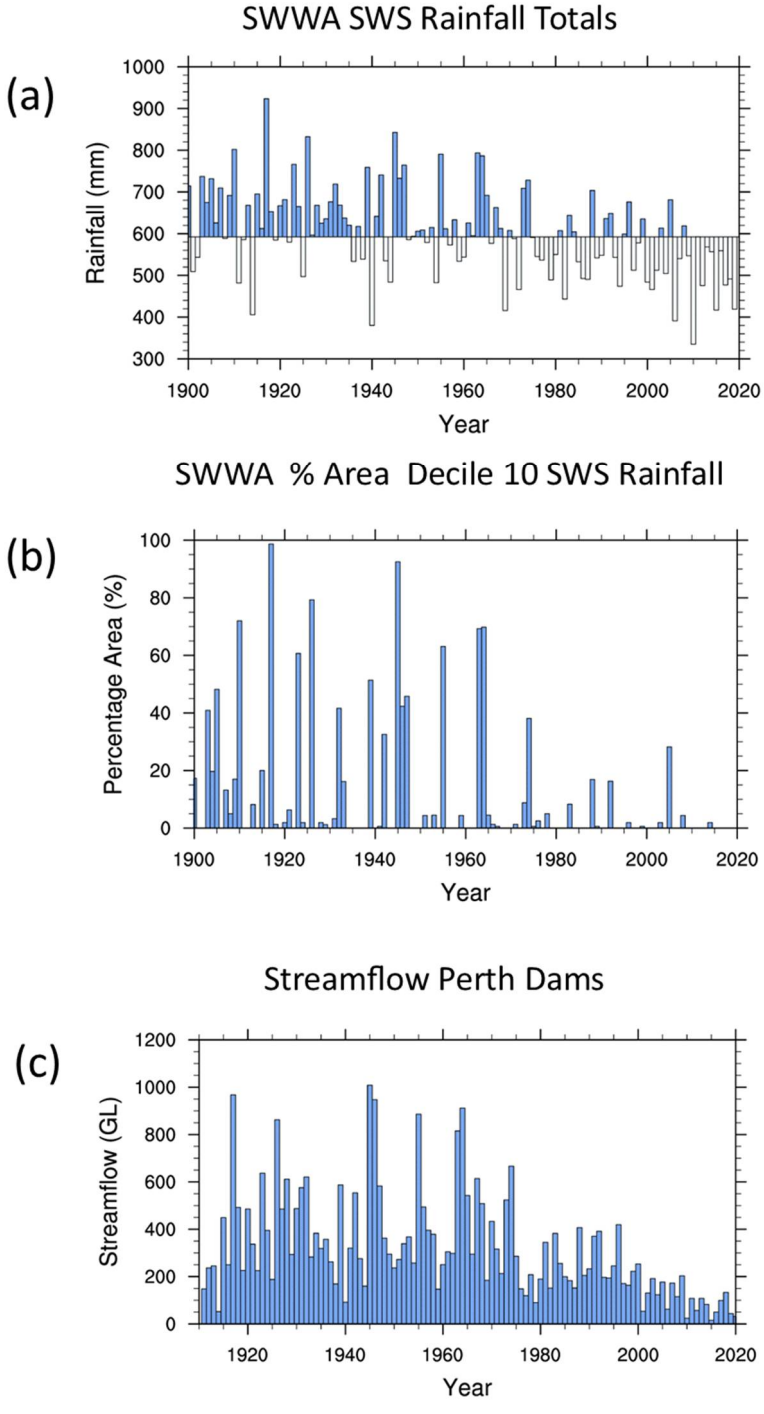

https://doi.org/10.5194/wcd-2021-72
Preprint. Discussion started: 15 November 2021


Figure 3

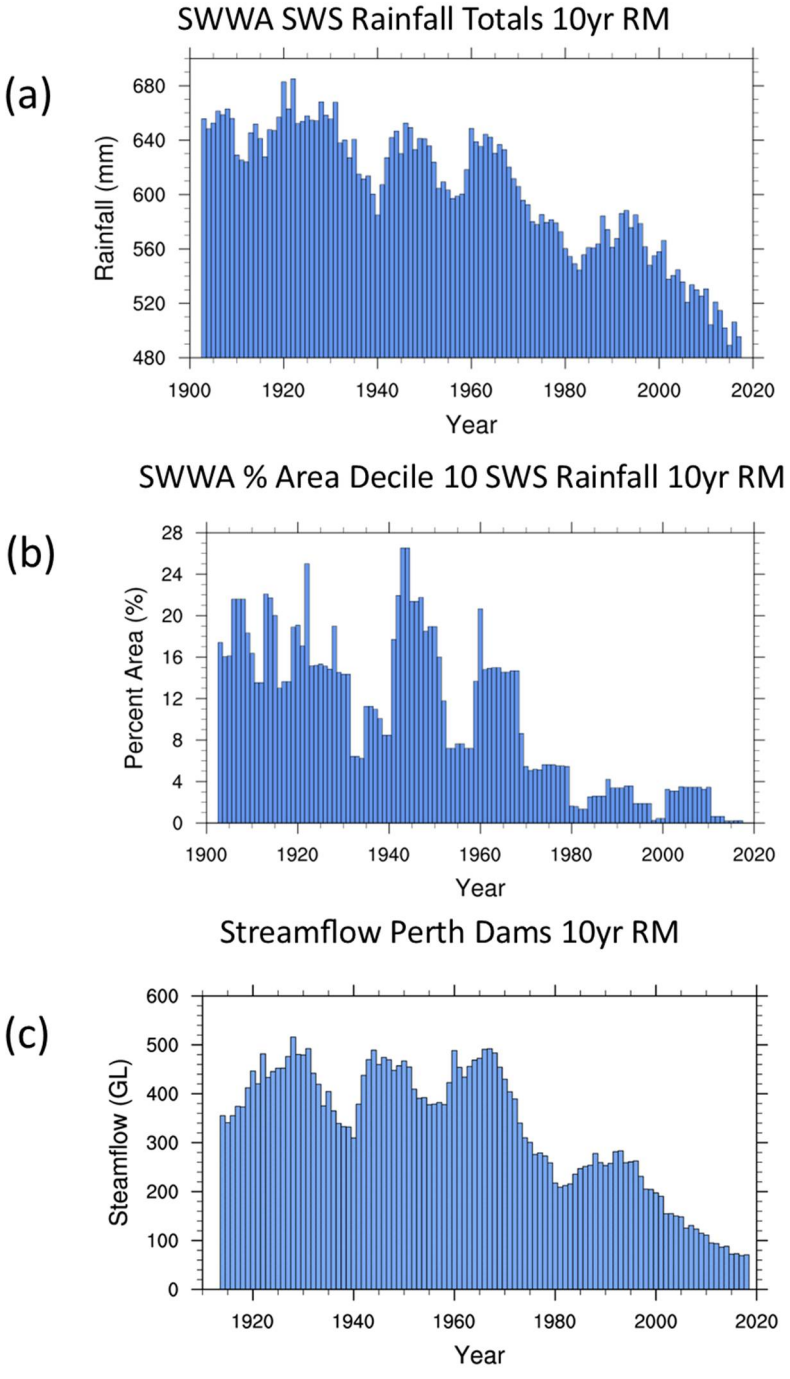


615

https://doi.org/10.5194/wcd-2021-72
Preprint. Discussion started: 15 November 2021


Figure 4

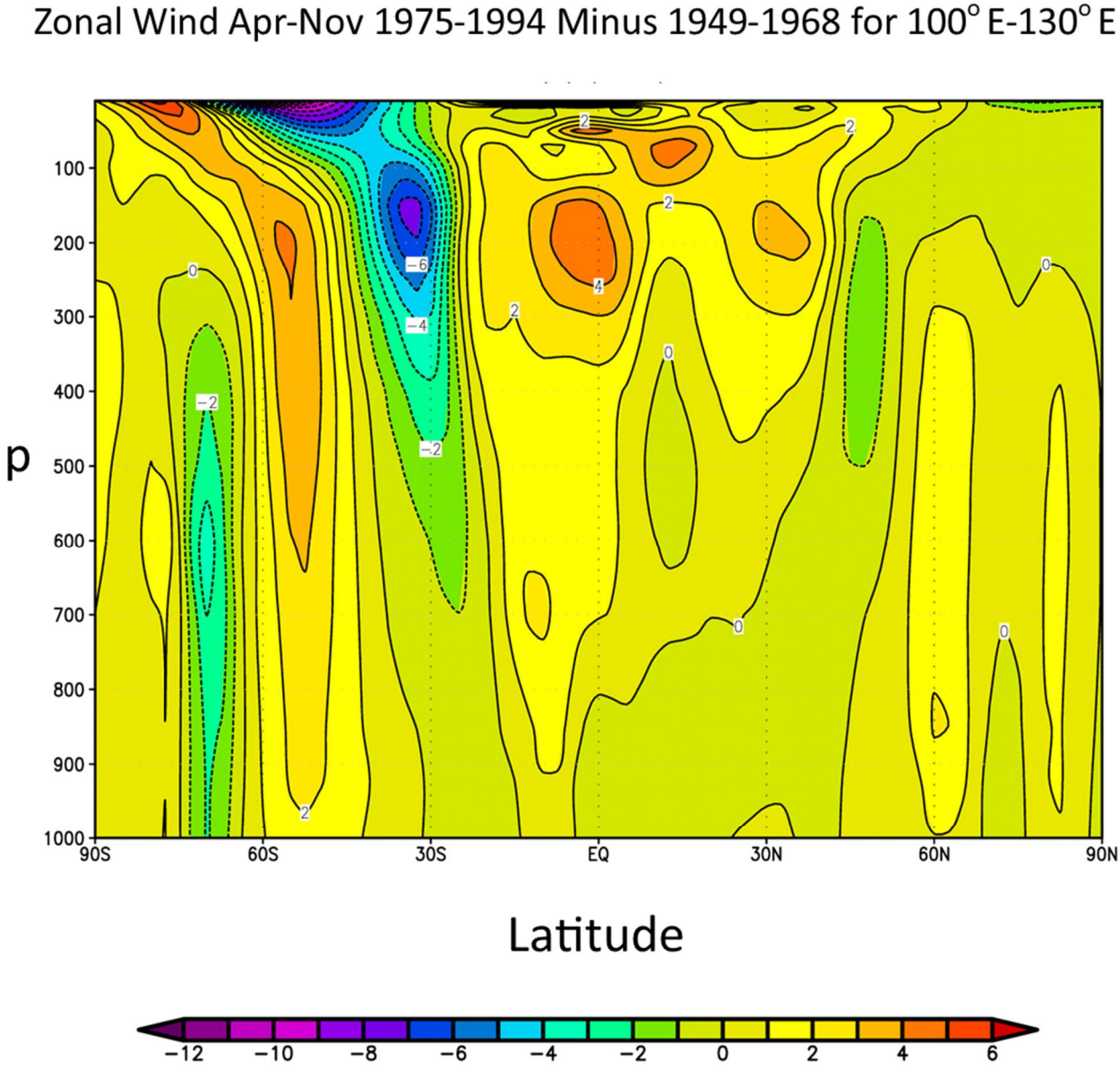


620

https://doi.org/10.5194/wcd-2021-72
Preprint. Discussion started: 15 November 2021


Figure 5

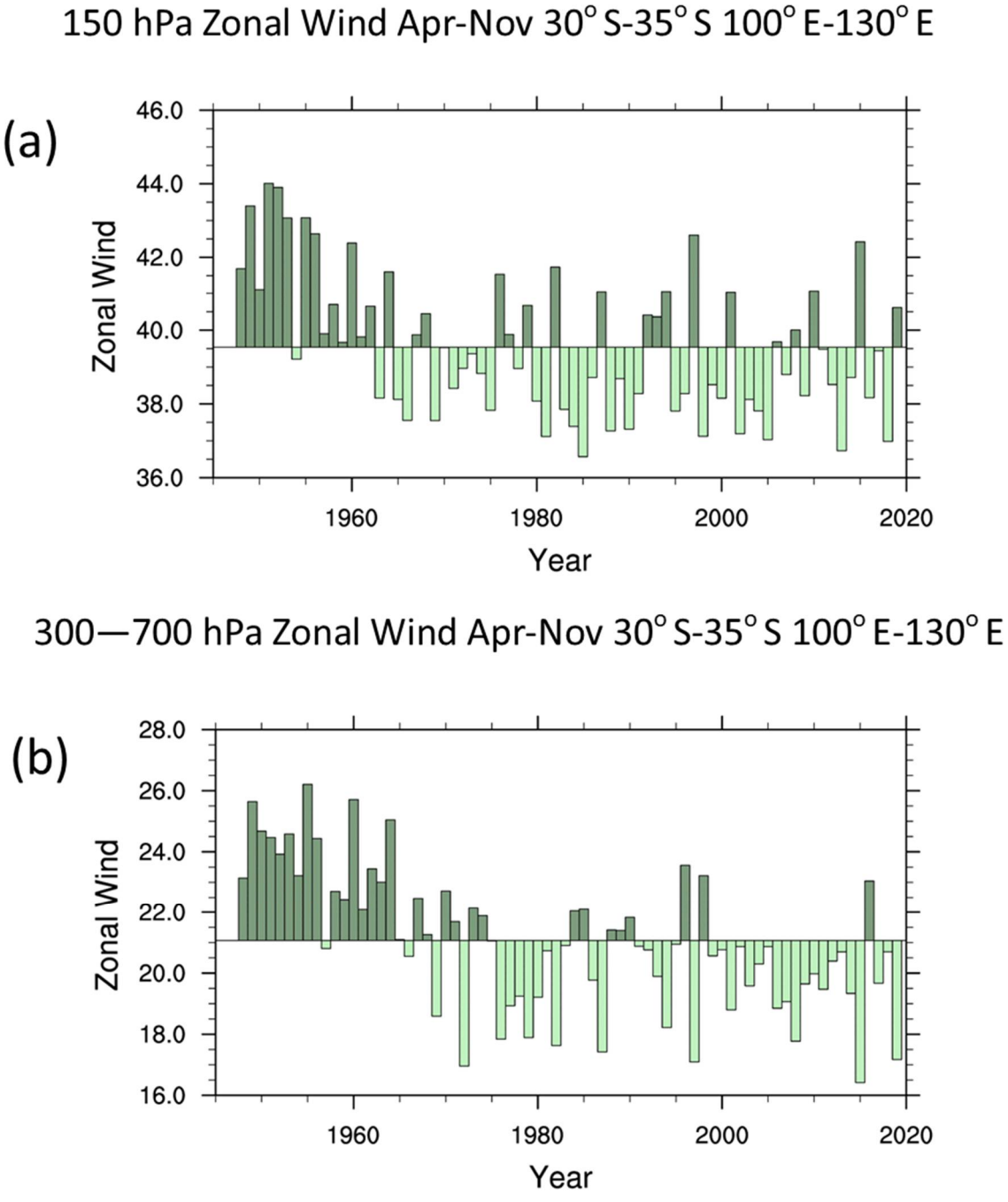

https://doi.org/10.5194/wcd-2021-72
Preprint. Discussion started: 15 November 2021




625 Figure 6

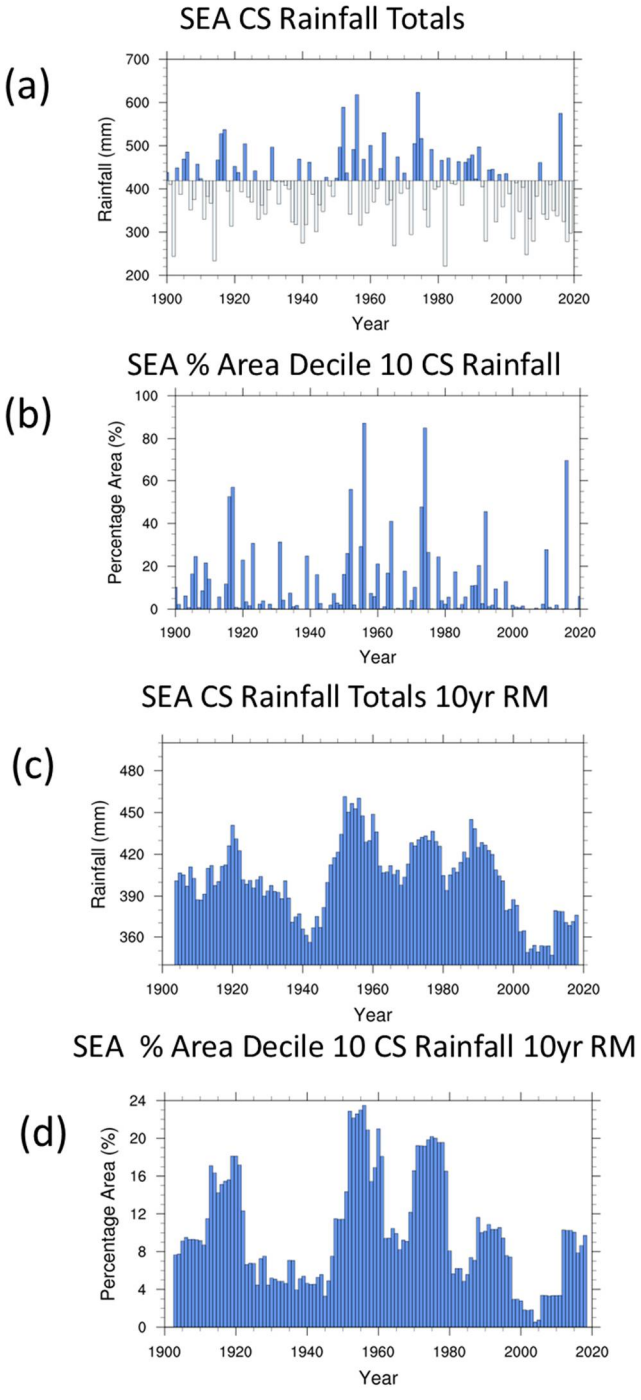

https://doi.org/10.5194/wcd-2021-72
Preprint. Discussion started: 15 November 2021


Figure 7

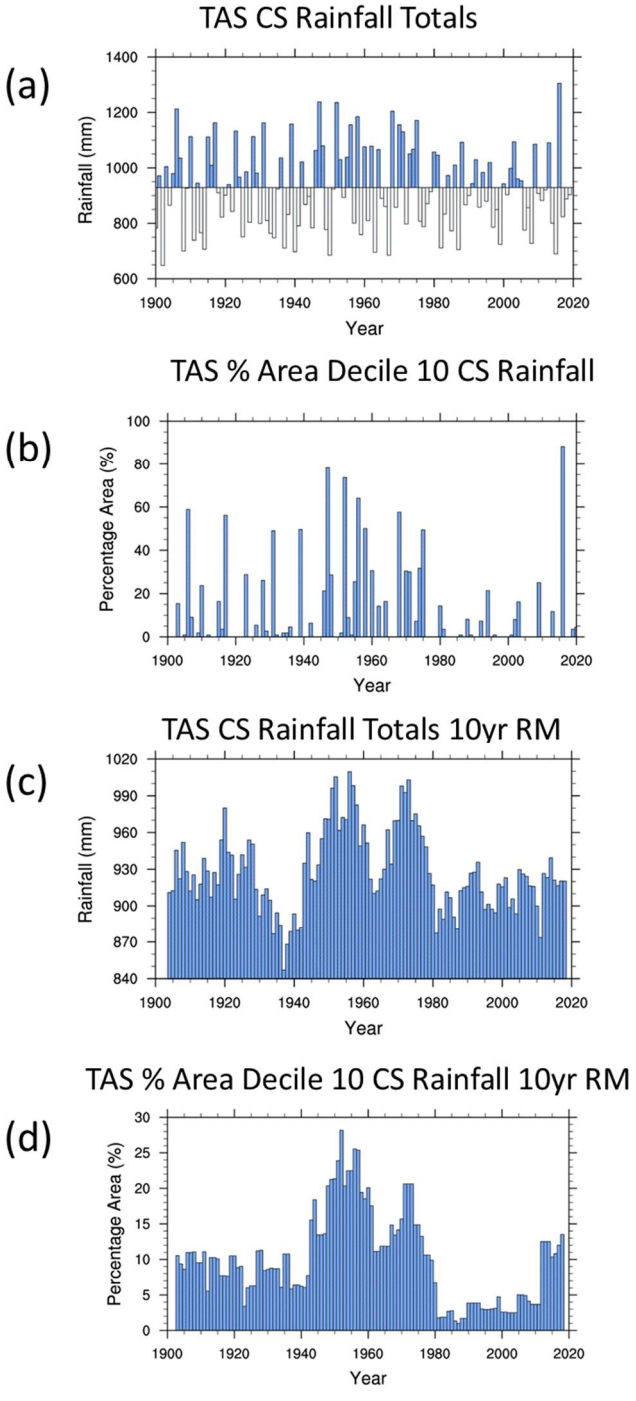

https://doi.org/10.5194/wcd-2021-72
Preprint. Discussion started: 15 November 2021


Figure 8

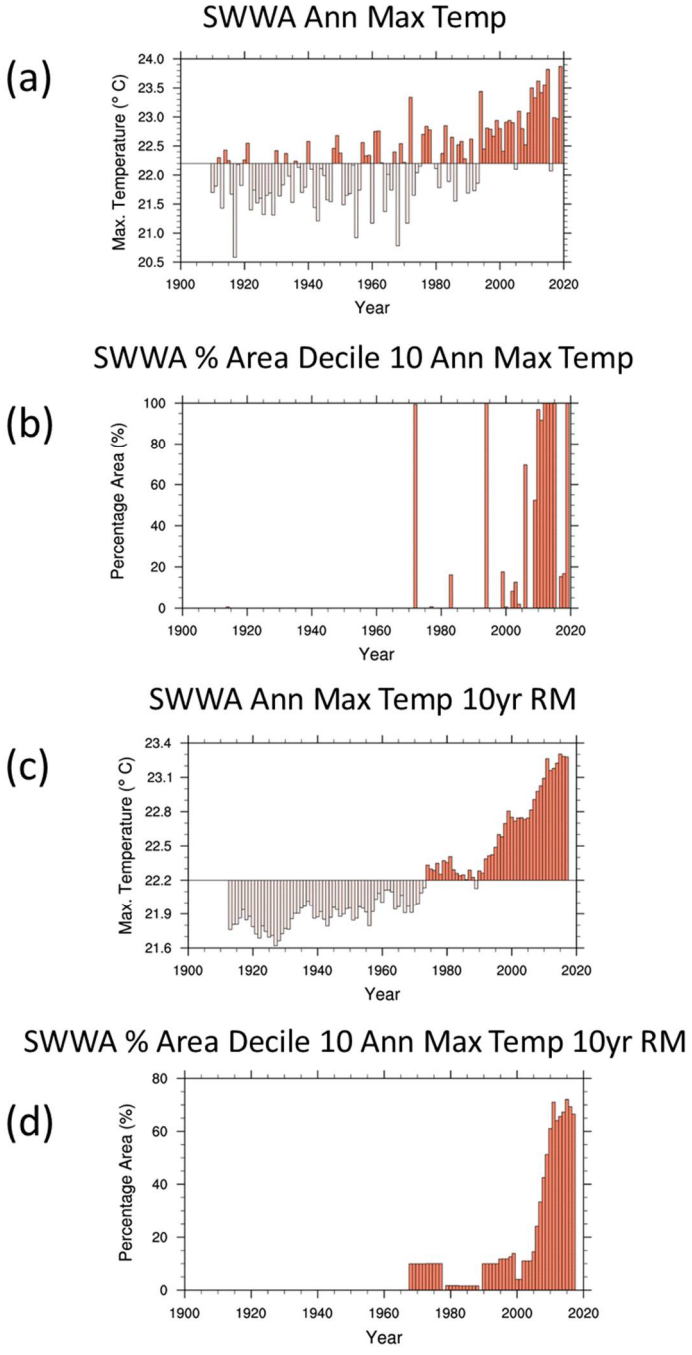


635

https://doi.org/10.5194/wcd-2021-72
Preprint. Discussion started: 15 November 2021


Figure 9

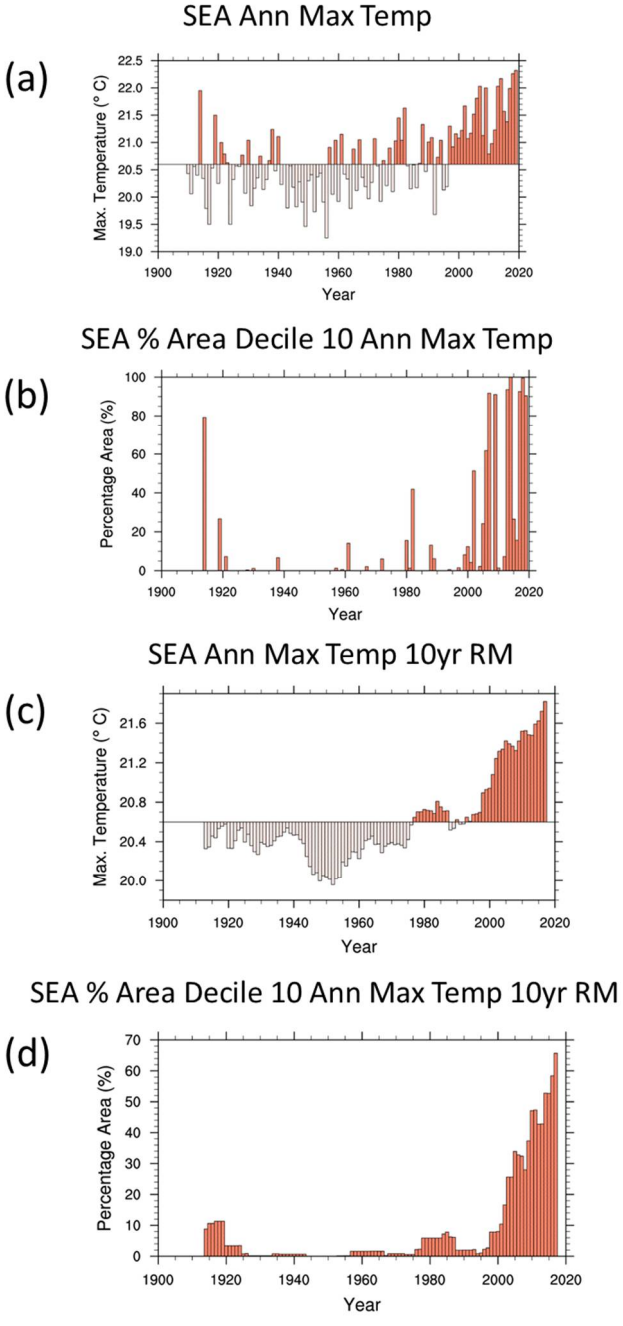


640

https://doi.org/10.5194/wcd-2021-72
Preprint. Discussion started: 15 November 2021


Figure 10